Peer-reviewed version available at Remote Sens. 2018, 10, 1102; doi:10.3390/rs10071102

Article

Vertically resolved precipitation intensity retrieved through a synergy between the ground-based NASA MPLNET lidar network measurements, surface disdrometer datasets and an analytical model solution

Simone Lolli [1,2,*], Leo Pio D'Adderio [3,4], James R. Campbell[5], Michäel Sicard [6,7], Ellsworth J. Welton[9], Andrea Binci[10], Alessandro Rea[11], Ali Tokay[2], Adolfo Comerón [6], Ruben Barragan [6,7], Jose Maria Baldasano [8], Sergi Gonzalez [12,13], Joan Bech [12], Nicola Afflitto [1], Jasper R. Lewis[2]

1 CNR-IMAA, Consiglio Nazionale delle Ricerche, Contrada S. Loja snc, Tito Scalo, PZ, Italy; simone.lolli@cnr.it
2 JCET-UMBC, University of Maryland Baltimore County, Baltimore, MD, USA; slolli@umbc.edu
3 CNR-ISAC, Consiglio Nazionale delle Ricerche, Roma, Via del Fosso del Cavaliere, 100,Roma RM, Italy
4 Università degli Studi di Ferrara, Dipartimento di Fisica, Via Saragat 1, Ferrara, FE, Italy
5 Naval Research Laboratory, Monterey, CA, 93940, USA
6 CommSensLab, Dept of Signal Theory and Communications, Universitat Politècnica de Catalunya, Barcelona, Spain
7 Ciències i Tecnologies de l'Espai - Centre de Recerca de l'Aeronàutica i de l'Espai / Institut d'Estudis Espacials de Catalunya (CTE-CRAE / IEEC), Universitat Politècnica de Catalunya, Barcelona, Spain
8 Environmental Modeling Laboratory, Universitat Politècnica de Catalunya, Barcelona, Spain
9 NASA GSFC, Code 612, Greenbelt, MD, 20771, USA
10 Università degli Studi di Roma III, Rome, Italy
11 GRASI S.r.l., Via Tumoli, 03100 Frosinone, Italy
12 Department of Applied Physics – Meteorology, University of Barcelona, Spain
13 Meteorological Surveillance and Forecasting Group, DT Catalonia, Agencia Estatal de Meteorología (AEMET), Barcelona, Spain
* Correspondence: simone.lolli@cnr.it; Tel.: +39-0971-427250

Abstract: In this paper we illustrate a new, simple and complementary ground-based methodology to retrieve the vertically resolved atmospheric precipitation intensity through a synergy between measurements from the National Aeronautics and Space Administration (NASA) Micropulse Lidar network (MPLNET), an analytical model solution and ground-based disdrometer measurements. The presented results are obtained at two mid-latitude MPLNET permanent observational sites, located respectively at NASA Goddard Space Flight Center, USA, and at the Universitat Politècnica de Catalunya, Barcelona, Spain. The methodology is suitable to be applied to existing and/or future lidar/ceilometer networks with the main objective of either providing near-real time (3h latency) rainfall intensity measurements and/or to validate satellite missions, especially for critical light precipitation (<3 mm hr^{-1}).

Keywords: rainfall; lidar; disdrometer; evaporation; meteorology; climate change; latent heat; precipitation

1. Introduction

Rain and precipitation influence the life of all living species on Earth. With respect to the Earth-Atmosphere system, they play a relevant role in pairing water and energy Earth's cycles serving as proxy for latent heat in the atmosphere. In fact, precipitation, modulating the latent heat content in the atmosphere [1], also modifies the atmospheric column thermodynamics, affecting cloud lifetime. [2]. Moreover, the hydrological cycle, which characterizes the continuous exchange of water in all

its three phases, below and above the earth surface, is clearly strongly dependent on precipitation. Then, characterizing rainfall intensity and its variability at global scale is crucial not only to improve our knowledge of the hydrological cycle but also to reduce uncertainties of global climate change model predictions of future scenarios. Understanding rainfall accumulation paths, together with their spatial variability, besides helping in identifying world regions subject to drought and flooding, is of fundamental importance in reducing global climate models uncertainty to forecasting global temperature change [3]. In this context and thanks to the technological progress in satellite remote sensing techniques, the National Aeronautics and Space Administration (NASA) launched jointly with the Japan Aerospace Exploration Agency (JAXA) the Tropical Rainfall Measuring Mission (TRMM) followed by the Global Precipitation Measurement (GPM) [1]. The main objective of TRMM missions was to monitor and study precipitation with satellite measurements in the tropics where two thirds of global precipitations occurs.

GPM further extended the measurement range towards the polar regions, (i.e., up to 69^o N/S). NASA is at the forefront of retrievals for vertically resolved microphysical rain drop properties from ground-based multi-wavelength lidar measurements [4] and their improvement through comparison with an analytical model solution that uses disdrometer and radiosounde data as inputs [5]. Taking advantage of the experience gained in these previous studies, we develop in this paper a new methodology to retrieve range-resolved rainfall intensity through a synergy between elastic lidar measurements, disdrometer data and an analytical model solution. Measurements obtained with this simple method, if implemented globally through existing or future lidar Level 2 algorithms and output datasets, will fill a gap to help validate satellite data for light precipitation (intensity <3 mm hr^{-1}) for which current global climate model predictions are in disagreement [1]. Results obtained from two mid-latitude NASA Micro Pulse Lidar NETwork (MPLNET [6]) permanent observational sites, one located at Goddard Space Flight Center (GSFC), USA, and the other at the Universitat Politècnica de Catalunya (UPC), Spain, are presented.

2. Materials and Methods

2.1. MPLNET lidar Data Measurements

The ground-based lidar systems used in this study are the elastic polarization-sensitive micro pulse lidar (P-MPL v. 4B, Sigma Space Corp., now LEICA) which are deployed at two permanent MPLNET lidar network observational sites. The purpose of NASA MPLNET network [6], active since 1999, is to retrieve automatically and continuously the geometrical and optical aerosol and cloud properties under most meteorological conditions and to the limit of laser signal attenuation. Measurements and retrievals obtained from worldwide deployed permanent stations are publicly available at MPLNET website. Multi-year network data were previously analyzed to assess cloud [7–10] and aerosol [2,11,12] radiative effects.

The P-MPL samples the atmosphere with a relatively high frequency (2500 Hz) using a low-energy (7 μJ) Nd:YAG laser at 532 nm. The P-MPL acquisition settings at the two sites focused upon in this study follow the NASA MPLNET temporal and spatial specifications (60s integration time and 75 m vertical resolution for GSFC and 60s and 30m for UPC). Polarization capabilities rely on the collection of two-channel measurements (i.e., the signal measured in the so-called 'co-polar' and 'cross-polar' channels of the instrument, respectively denoted as P_{co} (z) and P_{cr} (z). The total power, P, is reconstructed as $P = P_{co} + 2P_{cr}$ [13,14]). The signal, P, multiplied by the squared range is the basis for retrieving all of the different Level 2 cloud and aerosol products[15,16]. Since the P-MPL is a single wavelength lidar, however, the retrieval of the vertically-resolved microphysical and optical aerosol properties are subject to stronger assumptions with respect to multi-wavelength lidars [17]. For reference, these channels are not to be confused with traditional linear depolarization measurements, where co- and cross-polar channels represent those linear states with respect to the linearly-polarized

laser source (e.g., [18]). As introduced in [19], and given the engineering requirements and limitations of the MPL technique, the co-and cross-polar states are relative to non-linear phases.

Among the newly available MPLNET Version 3 (V3) release products, we consider the Level 1 V3 Cloud algorithm (beta product) [20], which automatically retrieves the cloud base height used to correctly reconstruct back the precipitating drop size distribution from the ground. The MPLNET systems used are those of the Universitat Politècnica de Catalunya (UPC), Barcelona, Spain, (41.38N, 2.11E, 115m a.s.l.) and of the Goddard Space Flight Center (GSFC), USA, (38.99N, 76.84W, 50m a.s.l.).

2.2. Disdrometer

The disdrometer is an in-situ measurement device designed to measure the drop size distribution (DSD;[21]), represented as the number of drops per unit of volume and per unit of raindrop diameter. Disdrometers can be based on different measurement principles (high-speed cameras, Doppler effect, laser-optical, impact, etc.). Two different versions Parsivel laser-optical disdrometer manufactured by OTT [22] are installed at UPC and GSFC, namely the first generation Parsivel (Parsivel^1) and the second generation Parsivel (Parsivel^2), respectively. Parsivel systems were originally developed by PM Tech Inc., Germany. The instrument has a laser diode (emitting wavelength of 780 nm) generating a horizontal flat beam. The measurement area is nominally 48 cm^2 for the first generation Parsivel and 54 cm^2 for Parsivel2. When a hydro-meteor passes through the laser beam, it produces attenuation proportional to its size. A relationship between the laser beam occlusion by the falling particle is applied to estimate the particle size. Parsivel instruments can measure particle diameters up to about 25 mm classifying them in 32 size classes of different width. The instrument also estimates the hydro-meter fall velocity by measuring the time necessary for the particle to pass through the laser beam, and thus it stores particles in 32x32 matrices. The disdrometers high temporal resolution (60s for this work) permits study in great detail of physical precipitation variability.

2.3. The Analytical Model Solution

The analytical model solution, based on molecular diffusivity of water vapor in air, permits calculating the *evaporation power* of a generic atmospheric layer in stationary thermodynamic conditions [23] through the variable D^*, which is the initial diameter of a raindrop that evaporates completely after traveling a certain distance in the incident atmospheric layer. Conversely, for our purposes, instead of D^*, we calculate the vertically resolved DSD profile at the radiosounding (or atmospheric model) vertical resolution [5]. The change in DSD diameter for each raindrop is calculated in the specific atmospheric layer starting from the altitude h_1 (ground) to the altitude h_2 (cloud base). The method reconstructs backwards the DSD atmospheric profile starting from the ground-based disdrometer DSD measurement to the cloud base height, at the resolution established by the corresponding atmospheric thermodynamic variables (i.e. temperature, mixing ratio...), as retrieved from the MPLNET lidar product [20]. If the radiosonde data are unavailable or too far from the measurement site, the atmospheric thermodynamics properties can be obtained from NASA Goddard Modeling and Assimilation Office, version 5.9.1 reanalysis (GEOS-5), available every 3 hours at each MPLNET station.

More specifically, we calculate how the raindrop diameter D_2 at altitude h_2 evolves into D_1 at altitude h_1 as through Eq.(1):

$$c_2 D_1^2 + c_1 D_2^2 = E(h_1, h_2), \tag{1}$$

, where the coefficients c_1 and c_2 are completely determined from the layer thermodynamic properties, h_1 and h_2 are the altitude boundaries of the specific layer while E is a function of the atmospheric layer status, i. e. humidity, temperature and pressure (see [23] for more detailed info).

For each range bin, at the radiosonde or GEOS-5 model resolution, the atmosphere is assumed to be steady, with constant thermodynamical variables. With such an assumption it is possible to reconstruct backward the DSD up to the cloud base. The primarily limitation of analytical model solution major limitation is that it does not take into account processes that affect raindrop diameter

such as coalescence and collision. For this reason, this method is more suitable for light intensity rainfalls, where those processes are not significant. Moreover, since the methodology further depends on lidar/ceilometer measurements, the rain intensity will affect the instrument Signal-to-Noise Ratio (SNR). Thus, the lidar/ceilometer signal will only be available up to the cloud base in light intensity rainfall given the potential limits of signal attenuation in heavier showers.

3. Results and Discussion

3.1. Seasonal differences at UPC

The UPC permanent observational site is located on the Remote Sensing Lab (RSlab) building in Barcelona, Spain. The disdrometer is deployed 600m away from the lidar at the meteorological observatory of the Applied Physics Department of the University of Barcelona. For this kind of application, such a short distance is not relevant in lighter rainfall and both instruments can be assumed as co-located. We analyzed the variability in seasonal rainfall intensity over 2016 where disdrometer and co-located MPLNET observations were simultaneously available. The largest rainfall events were found during the spring (March-April-May; MAM) and fall (September-October-November; SON) seasons. Rainfall intensity was analyzed at three different levels: 300m, 800m and 1300m above ground level (agl). During spring (Figure 1a), the peak of the distribution is shifted towards higher rainfall intensities (around 1.5 mm h^{-1}), while in fall (Figure 1b) the bulk of rainfall intensity is around 0.6 mm h^{-1}. This seasonal difference may be explained with different rain processes taking place (i.e., convective vs. stratiform events). There is no meaningful variability associated with different altitudes for both seasons. Due to the lower sample size measurements, the same analysis has not been performed at GSFC.

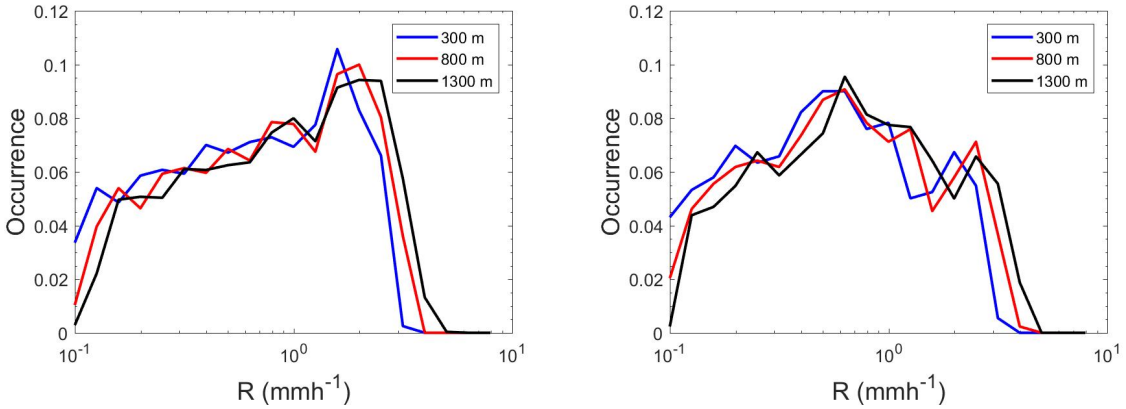

(a) Probability Density Function for rainfall events detected on 2016, Spring (March, April, May; MAM)

(b) Probability Density Function for rainfall events detected on 2016, Fall (September, October, November; SON)

Figure 1. Probability Distribution Function(PDF) for rainfall intensities at three vertical levels (300m, 800m, 1300m) during Spring (a) and Fall (b) 2016 at MPLNET Barcelona permanent observation station.

3.2. Case Study Analysis

Two case studies of the analytical model application at UPC and GSFC are presented and discussed in terms of vertically-resolved precipitation temporal evolution.

3.2.1. Retrieval of DSD profiles at UPC

On 04 April 2016, Fig. 2a shows the composite plot of the depolarized channel signal, where precipitation contours are visible at around 0900UT and from 1600UT to 1900UT. Fig. 2b shows the V3 L1 cloud algorithm cloud base height retrieval used in the inversion. Figure 2c depicts rainfall vertical intensity from 1940UT to 1950UT. Combining local radiosonde data (not showed here) and lidar data, we can state that rain originates from melting ice (cold rain process), with the freezing level detected at 2250m AGL, just a few tens of meters below the cloud base. This is also confirmed by GEOS-5 model (Fig. 2a), where 0°C isotherm is in very close agreement with radiosounding. In this rainfall event, the steepest gradient of intensity is 0.03 mm h^{-1} km^{-1}, which is much smaller than GSFC case study (see 3.2.2).

3.2.2. Retrieval of DSD profiles at GSFC

GSFC disdrometer and co-located lidar measurements were analyzed from November 2015 to April 2016. The vertical profiles of rainfall intensity, after applying the analytical model solution from 1727UT to 1754UT on 22 April 2016 , are showed Fig. 3. Depicted in 3a is depicted the composite plot of the depolarization channel signal obtained from the lidar on 22 April 2016. The core of the precipitation is clearly visible at around 1745UT. Figure 3b shows the cloud base height retrieval from V3 L1 MPLNET cloud algorithm. In Fig. 3c, we can observe that rainfall intensity is weak, but increasing with time. The steepest gradient with respect to altitude is recorded at 1747UT with 0.22 mm h^{-1} km^{-1}.

3.3. Evaporation Characteristics at UPC

In order to generalize the rain evaporation properties, UPC data measurements were analyzed as a function of rain parameter differences (i.e. R, the rain rate and Z, an equivalent radar reflectivity) between the cloud base and the ground. Figure 4a reports the analysis of R. The evaporation results are more marked (greater ΔR) for higher cloud base heights and increasing R values at the ground. For relatively high cloud bases (higher than 3000 m) the R difference with the ground reaches values as high as 6 mmh^{-1}. For lower R values and low cloud bases, ΔR is roughly constant, never exceeding 1 mmh^{-1}, regardless of the cloud base height. For lower cloud base heights (below 1000 m), ΔR is rain intensity insensitive at the ground and does not exceed 0.6-0.8 mmh^{-1}. Figure 4b shows Z properties, calculated as the sixth moment of the DSD. In contrast with R, the plot highlights that ΔZ is dependent only on the cloud base height. This can be explained, from a microphysical point of view, because of the small drop sizes collected in the analyzed data. That is, the lower the rain intensity, the smaller the drop diameters composing the DSD.

4. Conclusions

We introduce a methodology for computing vertically-resolved rain parameters (i. e., rain intensity) through a synergy between ground-based lidar, in-situ disdrometer measurements and an analytical model solution paired with thermodynamic variables measured by atmospheric radiosondes (if unavailable, atmosphere thermodynamic variables can be inferred from NASA GEOS-5 model). The methodology, applied at two permanent mid-latitude NASA Micro Pulse Lidar Network datasets, the Goddard Space Flight Center (GSFC) and Universitat Politècnica de Catalunya in Barcelona, Spain (UPC), is particularly suited for measurements of low intensity precipitation (rainfall rate, R, < 3 mm h^{-1}). If implemented operationally in the network, the methodology can generate near real time rainfall intensity as a standard Level 2 product. Low-intensity precipitation measurements are crucial for better understanding the hydrological cycle and for validating satellite missions, like the Global Precipitation Mission experiment (GPM) [1].

The analysis of a complete year (2016) of precipitation at UPC permitted assessing rainfall intensity seasonal variability for different cloud base altitude ranges. Slightly different rain intensity

Preprints (www.preprints.org) | NOT PEER-REVIEWED | Posted: 21 May 2018 doi:10.20944/preprints201805.0266.v1

Peer-reviewed version available at Remote Sens. 2018, 10, 1102; doi:10.3390/rs10071102

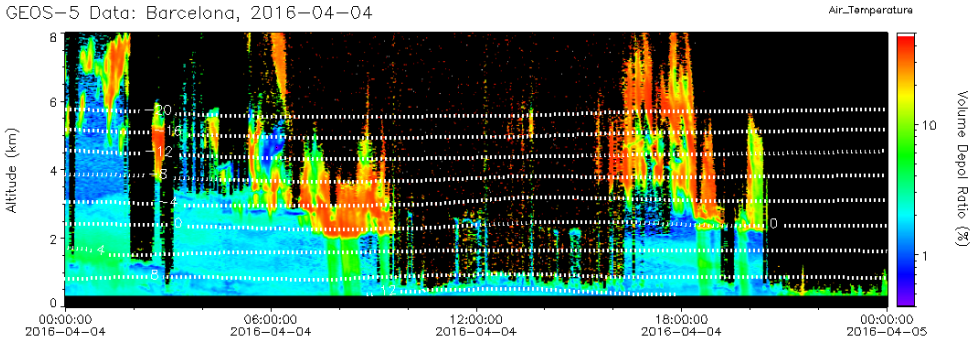

(a) Composite MPLNET V3 cross-polar channel with superimposed GEOS-5 isotherms

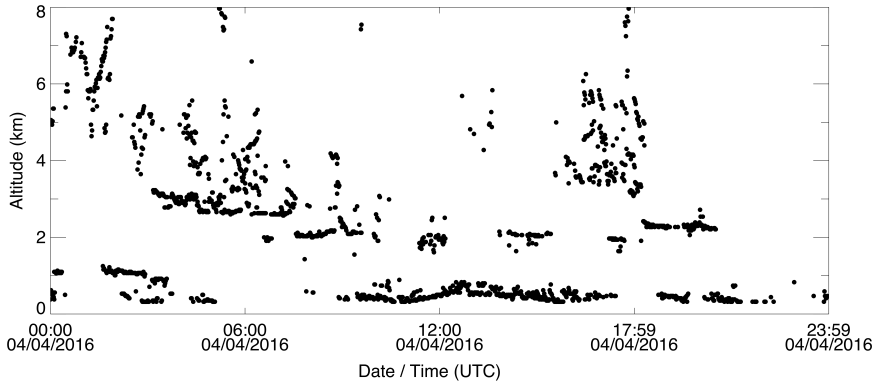

(b) MPLNET V3 L1 cloud base height retrieval product

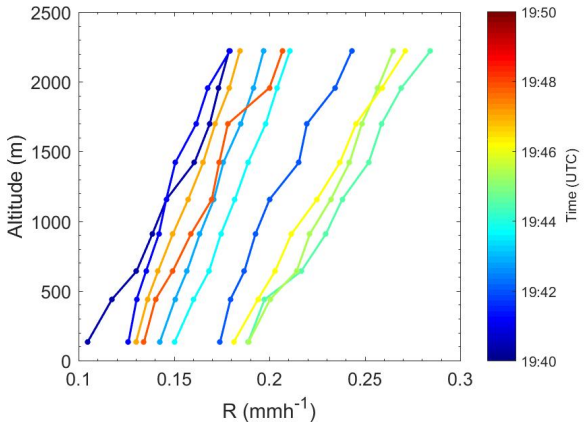

(c) Rainfall Intensity on 04 April 2016

Figure 2. Vertically-resolved rainfall intensity computations at different measurement times for UPC MPLNET station on 04 April 2016. (a) MPL cross-polar channel signal; (b) Cloud base height automatically retrieved by V3 L1 Cloud algorithm. (c) Vertically-resolved rainfall intensities, computed with the analytical model solution using disdrometer data and V3 L1 cloud base height retrieval, from 1940UT to 1950UT

distributions were observed during spring (MAM) and fall (SON), with a higher occurrence of relatively high rain rate during spring (1.5 vs. 0.6 mm h^{-1} mean R), and no dependence of the rain intensity with altitude. Yearly analysis of UPC MPLNET data shows that the effect of the evaporation on the rainfall

Preprints (www.preprints.org) | NOT PEER-REVIEWED | Posted: 21 May 2018 doi:10.20944/preprints201805.0266.v1

Peer-reviewed version available at Remote Sens. 2018, 10, 1102; doi:10.3390/rs10071102

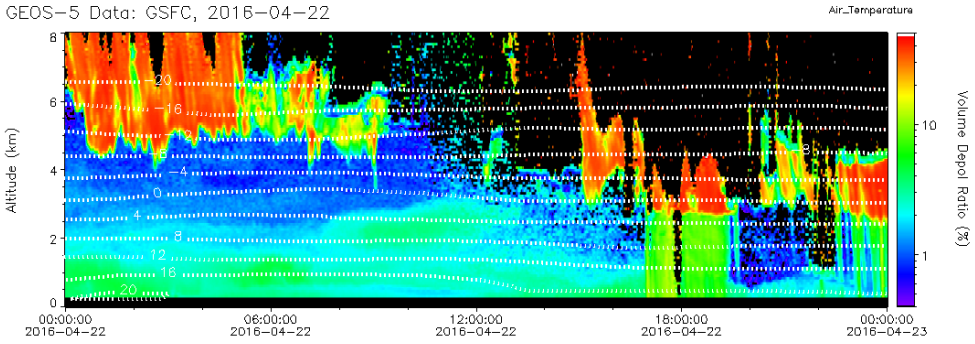

(a) Composite MPLNET V3 cross-polar channel with superimposed GEOS-5 isotherms

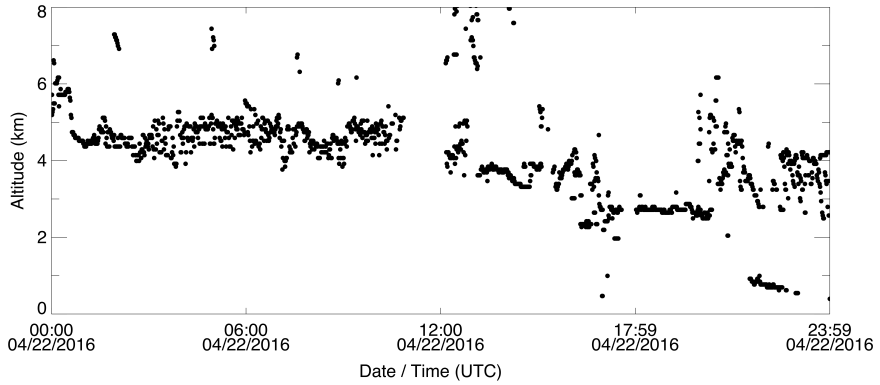

(b) MPLNET V3 L1 cloud algorithm cloud base retrieval product

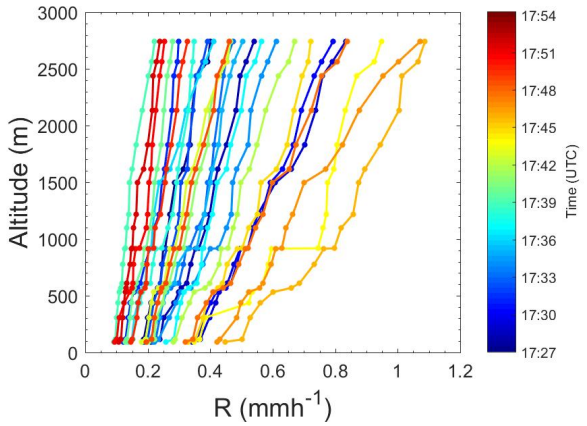

(c) Rainfall Intensity on 22 April 2016

Figure 3. Vertically-resolved rainfall intensity computations at different measurement times for the GSFC MPLNET station on 22 April 2016. (a) MPL cross-polar channel signal; (b) Cloud base height automatically retrieved by V3 L1 Cloud algorithm; (c) Vertically-resolved rainfall intensities, computed with the analytical model solution using disdrometer data and V3 L1 cloud base height retrieval, from 1727UT to 1754UT

rate has different impacts, depending on both rain intensity at ground and cloud base height. On the other hand, the radar reflectivity shows a dependence only on the cloud base height. The comparison between UPC and GSFC indicates that, for approximately the same rain intensity at the ground, the

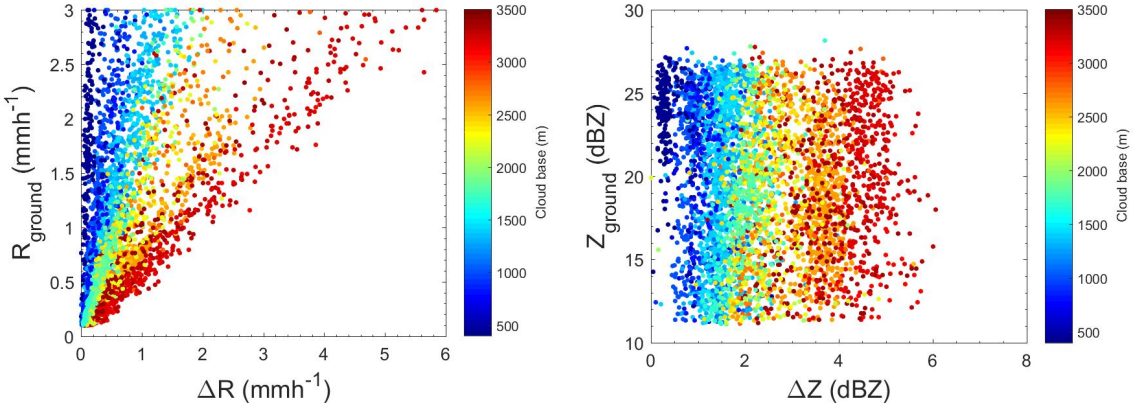

(a) Trend of ΔR as function of R at ground and cloud base height.

(b) Trend of ΔZ as function of R at ground and cloud base height.

Figure 4. Trend of the difference between the cloud base and the ground of the rain parameters R and Z as function of parameter values measured at ground and at cloud base height.

rain intensity gradients observed in GSFC (0.22 mm h^{-1} km^{-1}) are larger than the ones observed at UPC (0.03 mm h^{-1} km^{-1}). This result shows that, for this case study, the GSFC atmosphere is in general drier with respect to UPC.

Both analyzed case studies demonstrate the analytical model capability for reconstructing DSD from ground to cloud base. This also permits computing all of the significant distribution moments (i. e., radar reflectivity, liquid water content, mean mass diameter, etc.) besides rain reflectivity. Future research will focus on assessing light precipitation inter-annual intensity variability from long-term (>15 years) MPLNET stations, especially in polluted regions to quantifying for the first time the aerosol indirect effects on drizzle reduction/suppression.

Acknowledgments: S. Lolli would like to thank Dr. F. Madonna for constructive criticism of the manuscript. MPL measurements and processing in Barcelona are supported by the European Union (H2020, grant 654109, ACTRIS-2), the European Fund for Regional Development, the Spanish Government (grant TEC2015-63832-P, grants TEC2015-63832-P, CGL2015-65627-C3-2-R, CGL2016-81828-REDT) and the Catalan Government (grant 2014 SGR 583). CommSensLab is a Unidad de Excelencia María de Maeztu (grant MDM-2016-0600) funded by the Agencia Estatal de Investigación

References

1. Hou, A.Y.; Kakar, R.K.; Neeck, S.; Azarbarzin, A.A.; Kummerow, C.D.; Kojima, M.; Oki, R.; Nakamura, K.; Iguchi, T. The Global Precipitation Measurement Mission. *Bulletin of the American Meteorological Society* **2014**, *95*, 701–722.
2. Lolli, S.; Campbell, J.R.; Lewis, J.R.; Welton, E.J.; Di Girolamo, P.; Fatkhuroyan, F.; Gu, Y.; Marquis, J.W. Assessment of cirrus cloud and aerosol radiative effect in South-East Asia by ground-based NASA MPLNET lidar network data and CALIPSO satellite measurements. Remote Sensing of Clouds and the Atmosphere XXII. International Society for Optics and Photonics, 2017, Vol. 10424, p. 1042405.
3. Bosilovich, M.G.; Schubert, S.D.; Walker, G.K. Global Changes of the Water Cycle Intensity. *Journal of Climate* **2005**, *18*, 1591–1608.
4. Lolli, S.; Welton, E.J.; Campbell, J.R. Evaluating light rain drop size estimates from multiwavelength micropulse lidar network profiling. *Journal of Atmospheric and Oceanic Technology* **2013**, *30*, 2798–2807.
5. Lolli, S.; Di Girolamo, P.; Demoz, B.; Li, X.; Welton, E. Rain Evaporation Rate Estimates from Dual-Wavelength Lidar Measurements and Intercomparison against a Model Analytical Solution. *Journal of Atmospheric and Oceanic Technology* **2017**, *34*, 829–839.

6. Welton, E.J.; Campbell, J.R.; Spinhirne, J.D.; Scott, V.S. Global monitoring of clouds and aerosols using a network of micropulse lidar systems. Proc. SPIE, 2001, Vol. 4153, pp. 4153 – 4153 – 8.
7. Campbell, J.R.; Lolli, S.; Lewis, J.R.; Gu, Y.; Welton, E.J. Daytime cirrus cloud top-of-the-atmosphere radiative forcing properties at a midlatitude site and their global consequences. *Journal of Applied Meteorology and Climatology* **2016**, *55*, 1667–1679.
8. Lolli, S.; Campbell, J.R.; Lewis, J.R.; Gu, Y.; Marquis, J.W.; Chew, B.N.; Liew, S.C.; Salinas, S.V.; Welton, E.J. Daytime Top-of-the-Atmosphere Cirrus Cloud Radiative Forcing Properties at Singapore. *Journal of Applied Meteorology and Climatology* **2017**, *56*, 1249–1257.
9. Campbell, J.R.; Peterson, D.A.; Marquis, J.W.; Fochesatto, G.J.; Vaughan, M.A.; Stewart, S.A.; Tackett, J.L.; Lolli, S.; Lewis, J.R.; Oyola, M.I.; others. Unusually deep wintertime cirrus clouds observed over the alaskan sub-arctic. *Bulletin of the American Meteorological Society* **2017**.
10. Lolli, S.; Campbell, J.R.; Lewis, J.R.; Gu, Y.; Welton, E.J. Fu–Liou–Gu and Corti–Peter model performance evaluation for radiative retrievals from cirrus clouds. *Atmospheric Chemistry and Physics* **2017**, *17*, 7025–7034.
11. Pani, S.K.; Wang, S.H.; Lin, N.H.; Tsay, S.C.; Lolli, S.; Chuang, M.T.; Lee, C.T.; Chantara, S.; Yu, J.Y. Assessment of aerosol optical property and radiative effect for the layer decoupling cases over the northern South China Sea during the 7-SEAS/Dongsha Experiment. *Journal of Geophysical Research: Atmospheres* **2016**, *121*, 4894–4906.
12. Tosca, M.G.; Campbell, J.; Garay, M.; Lolli, S.; Seidel, F.C.; Marquis, J.; Kalashnikova, O. Attributing accelerated summertime warming in the southeast united states to recent reductions in aerosol burden: Indications from vertically-resolved observations. *Remote Sensing* **2017**, *9*, 674.
13. Campbell, J.R.; Hlavka, D.L.; Welton, E.J.; Flynn, C.J.; Turner, D.D.; Spinhirne, J.D.; III, V.S.S.; Hwang, I.H. Full-Time, Eye-Safe Cloud and Aerosol Lidar Observation at Atmospheric Radiation Measurement Program Sites: Instruments and Data Processing. *Journal of Atmospheric and Oceanic Technology* **2002**, *19*, 431–442.
14. Welton, E.J.; Campbell, J.R. Micropulse Lidar Signals: Uncertainty Analysis. *Journal of Atmospheric and Oceanic Technology* **2002**, *19*, 2089–2094.
15. Welton, E.J.; Voss, K.J.; Gordon, H.R.; Maring, H.; Smirnov, A.; Holben, B.; Schmid, B.; Livingston, J.M.; Russell, P.B.; Durkee, P.A.; others. Ground-based lidar measurements of aerosols during ACE-2: Instrument description, results, and comparisons with other ground-based and airborne measurements. *Tellus B* **2000**, *52*, 636–651.
16. Welton, E.J.; Voss, K.J.; Quinn, P.K.; Flatau, P.J.; Markowicz, K.; Campbell, J.R.; Spinhirne, J.D.; Gordon, H.R.; Johnson, J.E. Measurements of aerosol vertical profiles and optical properties during INDOEX 1999 using micropulse lidars. *Journal of Geophysical Research: Atmospheres* **2002**, *107*, INX2 18–1–INX2 18–20. 8019.
17. Lolli, S.; Madonna, F.; Rosoldi, M.; Campbell, J.R.; Welton, E.J.; Lewis, J.R.; Gu, Y.; Pappalardo, G. Impact of varying lidar measurement and data processing techniques in evaluating cirrus cloud and aerosol direct radiative effects. *Atmospheric Measurement Techniques* **2018**, *11*, 1639.
18. Sassen, K.; Knight, N.C.; Takano, Y.; Heymsfield, A.J. Effects of ice-crystal structure on halo formation: cirrus cloud experimental and ray-tracing modeling studies. *Appl. Opt.* **1994**, *33*, 4590–4601.
19. Flynn, C.J.; Mendoza, A.; Zheng, Y.; Mathur, S. Novel polarization-sensitive micropulse lidar measurement technique. *Opt. Express* **2007**, *15*, 2785–2790.
20. Lewis, J.R.; Campbell, J.R.; Welton, E.J.; Stewart, S.A.; Haftings, P.C. Overview of MPLNET Version 3 Cloud Detection. *Journal of Atmospheric and Oceanic Technology* **2016**, *33*, 2113–2134.
21. D'Adderio, L.; Porcù, F.; Tokay, A. Evolution of drop size distribution in natural rain. *Atmospheric Research* **2018**, *200*, 70–76.
22. Löffler-Mang, M.; Joss, J. An Optical Disdrometer for Measuring Size and Velocity of Hydrometeors. *Journal of Atmospheric and Oceanic Technology* **2000**, *17*, 130–139.
23. Li, X.; Srivastava, R.C. An Analytical Solution for Raindrop Evaporation and Its Application to Radar Rainfall Measurements. *Journal of Applied Meteorology* **2001**, *40*, 1607–1616.